

Improved Detection of Severe Storms Using Experimental Fine-Resolution WSR-88D Measurements

RODGER A. BROWN

NOAA/National Severe Storms Laboratory, Norman, Oklahoma

BRADLEY A. FLICKINGER, EDDIE FORREN, AND DAVID M. SCHULTZ

NOAA/National Severe Storms Laboratory, and Cooperative Institute for Mesoscale Meteorological Studies, University of Oklahoma, Norman, Oklahoma

DALE SIRMANS

RS Information Systems, Inc., Norman, Oklahoma

PHILLIP L. SPENCER

NOAA/National Severe Storms Laboratory, and Cooperative Institute for Mesoscale Meteorological Studies, University of Oklahoma, Norman, Oklahoma

VINCENT T. WOOD AND CONRAD L. ZIEGLER

NOAA/National Severe Storms Laboratory, Norman, Oklahoma

(Manuscript received 6 February 2004, in final form 16 June 2004)

ABSTRACT

Doppler velocity and reflectivity measurements from Weather Surveillance Radar-1988 Doppler (WSR-88D) radars provide important input to forecasters as they prepare to issue short-term severe storm and tornado warnings. Current-resolution data collected by the radars have an azimuthal spacing of 1.0° and range spacing of 1.0 km for reflectivity and 0.25 km for Doppler velocity and spectrum width. To test the feasibility of improving data resolution, National Severe Storms Laboratory's test bed WSR-88D (KOUN) collected data in severe thunderstorms using 0.5° -azimuthal spacing and 0.25-km-range spacing, resulting in eight times the resolution for reflectivity and twice the resolution for Doppler velocity and spectrum width. Displays of current-resolution WSR-88D Doppler velocity and reflectivity signatures in severe storms were compared with displays showing finer-resolution signatures. At all ranges, fine-resolution data provided better depiction of severe storm characteristics. Eighty-five percent of mean rotational velocities derived from fine-resolution mesocyclone signatures were stronger than velocities derived from current-resolution signatures. Likewise, about 85% of Doppler velocity differences across tornado and tornadic vortex signatures were stronger than values derived from current-resolution data. In addition, low-altitude boundaries were more readily detected using fine-resolution reflectivity data. At ranges greater than 100 km, fine-resolution reflectivity displays revealed severe storm signatures, such as bounded weak echo regions and hook echoes, which were not readily apparent on current-resolution displays. Thus, the primary advantage of fine-resolution measurements over current-resolution measurements is the ability to detect stronger reflectivity and Doppler velocity signatures at greater ranges from a WSR-88D.

1. Introduction

Doppler velocity and reflectivity measurements from Weather Surveillance Radar-1988 Doppler (WSR-88D) radars provide important input to forecasters as they

prepare to issue short-term severe storm and tornado warnings. As such, it is important that the radar provide as detailed information as possible, in both space and time. Toward this end, a new scanning strategy (Volume Coverage Pattern 12) is being added to WSR-88D radars to provide finer temporal resolution and finer vertical resolution at lower elevation angles (e.g., Brown et al. 2003). An approach is discussed in this paper for increasing horizontal resolution as well.

Corresponding author address: Dr. Rodger A. Brown, National Severe Storms Laboratory, 1313 Halley Circle, Norman, OK 73069.

E-mail: Rodger.Brown@noaa.gov

WSR-88Ds collect full-resolution base data (reflectivity, Doppler velocity, spectrum width) with an azimuthal spacing of 1.0° and range spacing of 0.25 km. Doppler velocity and spectrum width are recorded and displayed at this spacing. However, full-resolution reflectivity (received power) measurements are averaged over four range intervals and are recorded and displayed at coarser 1.0-km intervals (Fig. 1). Many severe storm reflectivity signatures (e.g., gust fronts, hook echoes, bounded weak echo regions) would be identifiable at farther ranges if full 0.25-km spacing were displayed.

Through use of Doppler velocity simulations, Wood et al. (2001) and Brown et al. (2002) have shown that finer azimuthal spacing could result in stronger Doppler velocity signatures of mesocyclones and tornadoes, respectively. Their simulations reveal that, if WSR-88D measurements were made at azimuthal sampling intervals of 0.5° instead of current intervals of 1.0° , signatures would be detectable 50% farther in range. Furthermore, they used experimental time series data collected by the WSR-88D Radar Operations Center's test bed KCRI radar in Norman, Oklahoma, during the 3 May 1999 Oklahoma–Kansas tornado outbreak to confirm that stronger Doppler velocity signatures arise from 0.5° -azimuthal sampling.

To help reinforce these findings, the National Severe Storms Laboratory's (NSSL) test bed WSR-88D radar (KOUN) collected fine-resolution data on severe thunderstorm days during spring 2003. The procedure was to record fine-resolution base data at 0.5° azimuthal spacing and 0.25-km range spacing (Fig. 1). Then a recombination algorithm (e.g., Curtis et al. 2003) was used to produce the lower-resolution data (1.0° , 1 km

for reflectivity and 1.0° , 0.25 km for Doppler velocity and spectrum width) that are currently recorded and displayed by WSR-88Ds. A study is underway at NSSL to determine whether the recombination approach is adequate for operational applications.

In this study, we compared Doppler velocity and reflectivity signatures found on the fine-resolution displays (0.5° , 0.25 km) with those on the current-resolution displays. Eighty-five percent of mean rotational velocities for mesocyclones derived from fine-resolution mesocyclone signatures were stronger than velocities derived from current-resolution signatures. Doppler velocity differences across tornado and tornadic vortex signatures showed similar improvements. On fine-resolution displays, low-altitude boundaries were more readily apparent. At ranges greater than 100 km, fine-resolution reflectivity displays revealed severe storm signatures, such as bounded weak echo regions and hook echoes, that were not readily apparent on current-resolution displays. An advantage of fine-resolution measurements over current-resolution measurements is the ability to detect stronger reflectivity and Doppler velocity signatures at greater ranges from a WSR-88D.

2. Data

During spring 2003, NSSL's KOUN radar was devoted to collecting data for the Joint Polarization Experiment (JPOLE; e.g., Schuur et al. 2004). JPOLE personnel agreed to modify their scanning strategies to accommodate fine-resolution data collection, while at the same time separately recording current-resolution dual-polarization data for their study.

Since the same antenna rotation rate was used for both current- and fine-resolution data, half the number of pulses was utilized to produce the fine-resolution data. With half the number of pulses, the standard deviations of the mean Doppler velocity and reflectivity estimates increase by $\sqrt{2}$ or 1.4. For current 1.0° azimuthal sampling, WSR-88D system specifications require that, for an input spectrum width of 4 m s^{-1} , signal-to-noise ratio greater than 10 dB, and antenna rotation rates less than 28° s^{-1} , the system delivers a standard deviation of 1.0 m s^{-1} or less for the mean Doppler velocity estimate and a standard deviation of 1 dB or less for the reflectivity estimate (e.g., Heiss et al. 1990). These conditions apply for contiguous waveforms at all pulse repetition frequencies (PRF). For 0.5° azimuthal sampling, the system specifications deliver standard deviations of 1.4 m s^{-1} and 1.4 dB or less, respectively, for mean Doppler velocity and reflectivity estimates.

The two primary JPOLE scanning strategies, A and B, used in this study are shown in the appendix. For strategy A, 0.5° Doppler velocity estimates have a standard deviation of 1.27 m s^{-1} and for B the standard

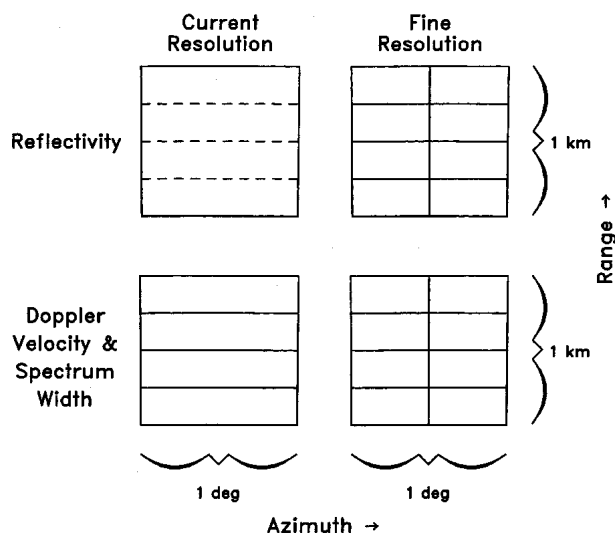


FIG. 1. Size of radar display elements (azimuth across page, range up page) for (left) current WSR-88D resolution and (right) fine-resolution data at a range of 60 km from a radar. Dashed lines in current reflectivity box (1° by 1 km) indicate that four full-resolution range bins are averaged to produce the current reflectivity value.

deviation is 1.19 m s^{-1} for the above system specifications. Low PRF reflectivity data have a standard deviation of 1.03 dB for both scanning strategies. High PRF reflectivity data have essentially the same standard deviation for both strategies A and B—1.48 versus 1.45 dB. These standard deviations for JPOLE scanning strategies are slightly greater (4%) than those that would be expected with an operational fine-resolution version of WSR-88D VCP 11.

Since WSR-88D meteorological algorithms have not yet been modified to automatically identify reflectivity and Doppler velocity signatures for KOUN scanning strategies, signature identifications were performed manually. Both current- and fine-resolution data were analyzed using NSSL's Warning Decision Support System—Integrated Information (WDSS-II) displays (e.g., Hondl 2002). Doppler velocity characteristics of current- and fine-resolution signatures of mesocyclones and tornadoes were tabulated, while occurrences of pertinent reflectivity signatures were noted.

3. Comparisons of mesocyclone signatures

a. Simulations

As an introduction to comparisons of fine-resolution to current-resolution measurements in mesocyclones, we present some of the simulation results of Wood et al. (2001). A comparison of simulated Doppler radar scans across a model mesocyclone for 1.0° - and 0.5° -azimuthal sampling shows that mesocyclone signatures with 0.5° -azimuthal sampling are stronger (Fig. 2). The peaks of the measurement curve for 0.5° -azimuthal sampling (Fig. 2b) are closer to the pointed peaks of the “true” curve than are those for 1.0° sampling (Fig. 2a). The peaks for 0.5° sampling are closer to the true value because the radar beam has to scan only half the distance in azimuth and therefore the true curve is less smeared. Also, with 0.5° -azimuthal sampling there are twice as many data points along the measurement curve and therefore there is a greater probability that a data point will fall close to the peaks of the measurement curve. For the example in Fig. 2, the mean rotational velocity (average of the two extreme Doppler velocity data points) detected by 1.0° sampling is 16.2 m s^{-1} , whereas the mean rotational velocity detected by 0.5° sampling is 19.0 m s^{-1} —an increase of 17%.

The data points along each measurement curve in Fig. 2 represent the placement of data points for one scan of the radar through the mesocyclone; data points are separated by one azimuthal sampling interval (ΔAZ). From one scan to the next, placement of data points would be at different positions relative to the peaks of the measurement curve. To approximate a number of possible placements, Wood et al. (2001) computed mean rotational velocities for 51 dif-

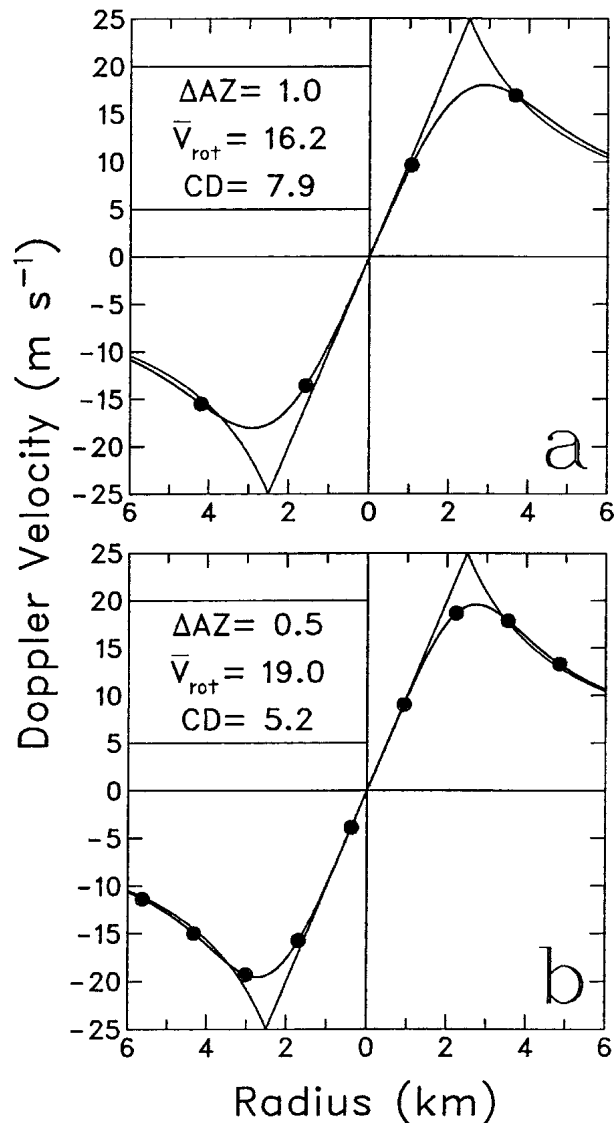


FIG. 2. Relationship of data points relative to the azimuthal profile of a mesocyclone signature for azimuthal sampling intervals (ΔAZ) of (a) 1.0° and (b) 0.5° at 150-km range. The measurement curve with rounded peaks (along which data points fall) represents the Doppler velocity azimuthal profile of the mesocyclone signature if the radar were able to make measurements in a continuous manner across the mesocyclone. Data points (black dots) represent locations of successive Doppler velocity measurements collected at ΔAZ intervals as the radar beam scans across the mesocyclone. The model (“true”) azimuthal profile is indicated by the curve with pointed peaks (Rankine combined vortex) corresponding to a typical mesocyclone having a peak rotational velocity of 25 m s^{-1} at a core diameter of 5 km. Values of mean rotational velocity (\bar{V}_{rot} , m s^{-1}) and core diameter (CD, km) deduced from measurements are indicated (from Wood et al. 2001).

ferent scans where data points were shifted in azimuth by $\Delta AZ/51$ from one scan to the next. To produce realistic computations, random noise then was added to individual data points before extreme values were se-

lected for the mean rotational velocity computations. Adding random noise is important because Doppler velocity measurements have an inherent uncertainty owing to the finite number of samples used to compute mean Doppler velocity values. For 0.5° -azimuthal data collection, the antenna was assumed to be rotating at the same speed as for 1.0° data collection and therefore half as many samples were collected. Random noise values added to the 0.5° -azimuthal data accordingly were 1.4 times greater than for 1.0° data (1.0 versus 0.7 m s^{-1}).

The resulting 51 mean rotational velocities are presented as frequency distributions at three different ranges (Fig. 3). The left and right distribution in each panel is the distribution of mean rotational velocities computed from 1.0° and 0.5° data, respectively. On average, data collected at 0.5° azimuthal intervals produce stronger mean rotational velocities for mesocyclones. However, there is an 11%–22% overlap of the two distributions among the three ranges displayed, indicating that on some occasions 1.0° data may produce stronger rotational velocities.

b. Radar data

Fine-resolution data were collected in Oklahoma mesocyclones on six days during spring 2003: 19 April, 24 April, 8 May, 10 May, 16 May, and 19 May. These data were then recombined into current WSR-88D resolution data (1.0° , $0.25/1.0 \text{ km}$) using the Curtis et al. (2003) approach. Doppler velocity displays of these datasets were visually inspected for mesocyclone signatures, and signature characteristics were tabulated. A total of 620 pairs of fine- and current-resolution signatures were found at various elevation angles on those six days.

Percentage differences between mean rotational velocities from 0.5° data and mean velocities from 1.0° data were computed (Fig. 4). Included in the figure are similar data collected during the Oklahoma–Kansas tornado outbreak of 3 May 1999 (Wood et al. 2001). As expected, based on Fig. 3, the vast majority (85%) of 0.5° mesocyclone signatures were stronger than 1.0° signatures, with 25% of the signatures being at least 10% stronger. About 15% of the 1.0° signatures were stronger, in general agreement with the overlapped portions of the simulated distributions in Fig. 3.

The data in Fig. 4, reinforced by simulation results in Fig. 3, indicate that forecasters would benefit from finer-resolution 0.5° data when issuing severe storm and tornado warnings, since mesocyclone signatures typically are stronger with 0.5° data collection. Being stronger, it may be argued that signatures exceed a given threshold value earlier in their lifetime and, as shown by the Wood et al. (2001) simulations, they continue to exceed the threshold value up to 50% farther in range.

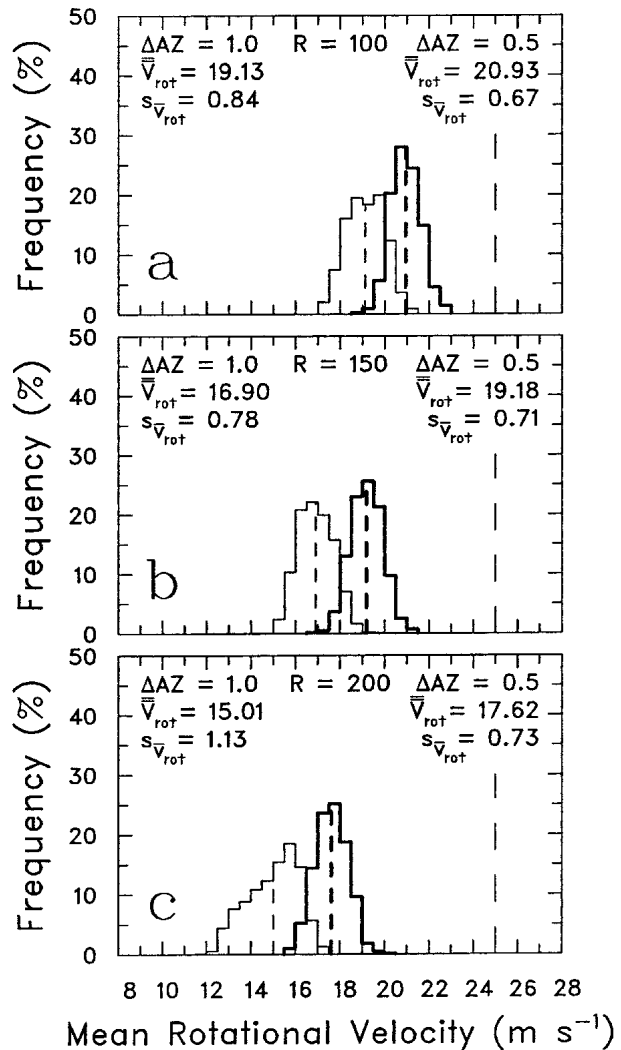


FIG. 3. Frequency distributions of mean rotational velocity estimates for a typical model mesocyclone (peak rotational velocity of 25 m s^{-1} , core diameter of 5 km) arising from chance placements of radar beams relative to peaks of the measurement curves (as in Fig. 2) at ranges of (a) 100, (b) 150, and (c) 200 km. Thin and thick lines correspond to 1.0° - and 0.5° -azimuthal data collection, respectively. Average of mean rotational velocity values (\bar{V}_{rot} , m s^{-1} ; vertical dashes) and standard deviation ($s_{\bar{V}_{\text{rot}}}$, m s^{-1}) of each distribution are indicated. As expected, the strength of a mesocyclone signature decreases with increasing range from the radar (i.e., with increasing width of the radar beam). Vertical dashed line to the right represents the mesocyclone's peak rotational velocity (after Wood et al. 2001).

4. Comparisons of tornado signatures

a. Simulations

Brown et al. (2002) simulated Doppler velocity measurements through four model tornadoes having a range of peak rotational velocities and core diameters. When the core diameter of a tornado is larger than the radar beamwidth, the resulting Doppler velocity signa-

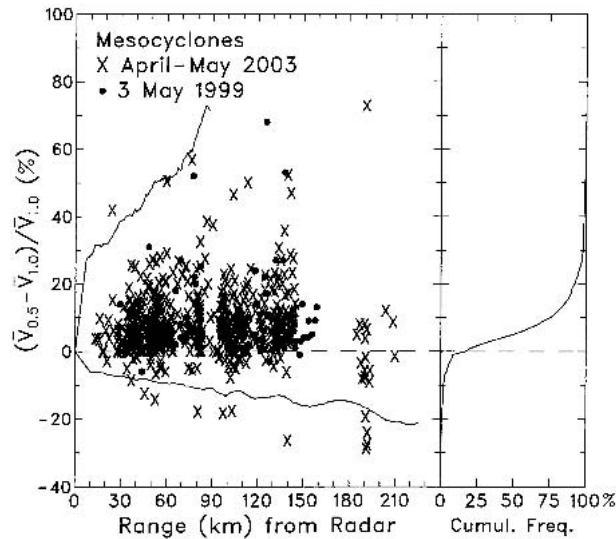


FIG. 4. Percentage differences between mesocyclone mean rotational velocities from 0.5°-azimuthal data collection and mean rotational velocities from 1.0°-azimuthal data collection at all elevation angles plotted as a function of range from radar. Each data point represents the percentage difference at a given elevation angle. A total of 620 points are plotted for Apr–May 2003 signatures and 91 points for 3 May 1999 signatures. Upper and lower curves represent likely extreme ratios based on simulations of Wood et al. (2001). Cumulative frequency distribution of number of data points is shown on the right side.

ture is called a *tornado signature* (e.g., Brown et al. 2002). On the other hand, when the core diameter is smaller than the width of the radar beam, a different type of Doppler velocity signature is produced. In such situations, Brown et al. (1978) showed that the extreme Doppler velocity values produce a signature (which they called a *tornadic vortex signature* or TVS) that is about one beamwidth in diameter regardless of size or strength of the tornado. TVS magnitude, however, is related to the size and strength of the tornado, but it is underestimated by some unknown amount because the actual size and strength of the tornado is unknown. Accordingly, the convention is to use the Doppler velocity difference across the signature to indicate signature magnitude, rather than using mean rotational velocity as is the case for mesocyclones.

Distributions of Doppler velocity difference (ΔV) for two of the Brown et al. (2002) model tornadoes are reproduced in Figs. 5 and 6. The distributions were computed the same way as for those shown in Fig. 3, but were based on 120 different scans, where data points were shifted in azimuth by $\Delta AZ/120$ from one scan to the next. Since tornado and tornadic vortex signatures are regions of high shear, standard deviations of random noise added to the 1.0° and 0.5° azimuthal data points were 2.5 and 3.5 m s^{-1} , respectively.

The distributions for the larger and stronger tornado D (Fig. 6) overlap by only 2%–9%, even at far range,

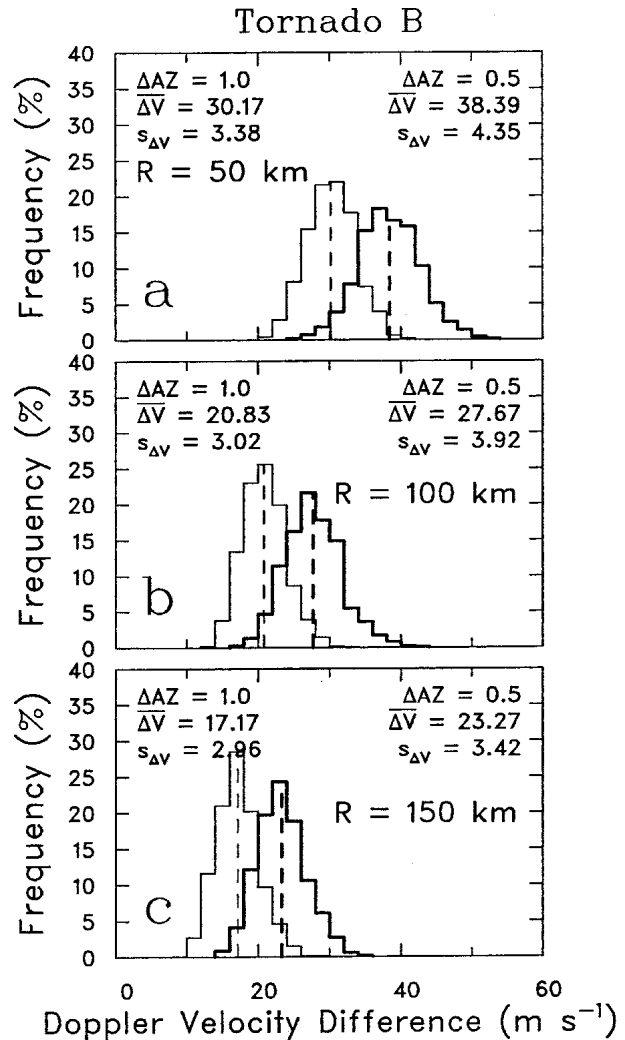


FIG. 5. Frequency distributions of Doppler velocity differences (ΔV) representing the full range of potential radar beam sampling positions relative to simulated tornado B (Rankine combined vortex with peak rotational velocity of 50 m s^{-1} and core diameter of 200 m) at ranges (R) of (a) 50, (b) 100, and (c) 150 km. Thin and thick lines correspond to azimuthal sampling intervals of 1.0° and 0.5°, respectively. The mean ($\overline{\Delta V}$, m s^{-1} ; vertical dashed line) and standard deviation ($s_{\Delta V}$, m s^{-1}) of each ΔV distribution are indicated (after Brown et al. 2002).

whereas the distributions for the smaller and weaker tornado B (Fig. 5) overlap by 25%–33%. Evidently, the advantage of 0.5°-azimuthal sampling decreases somewhat for smaller and weaker tornadoes like B. However, larger and stronger tornadoes like D, which cause the most damage and casualties, produce much stronger signatures with 0.5°-azimuthal sampling and maintain stronger signatures at all ranges.

b. Radar data

Percentage differences were computed between Doppler velocity differences with 0.5°-azimuthal sam-

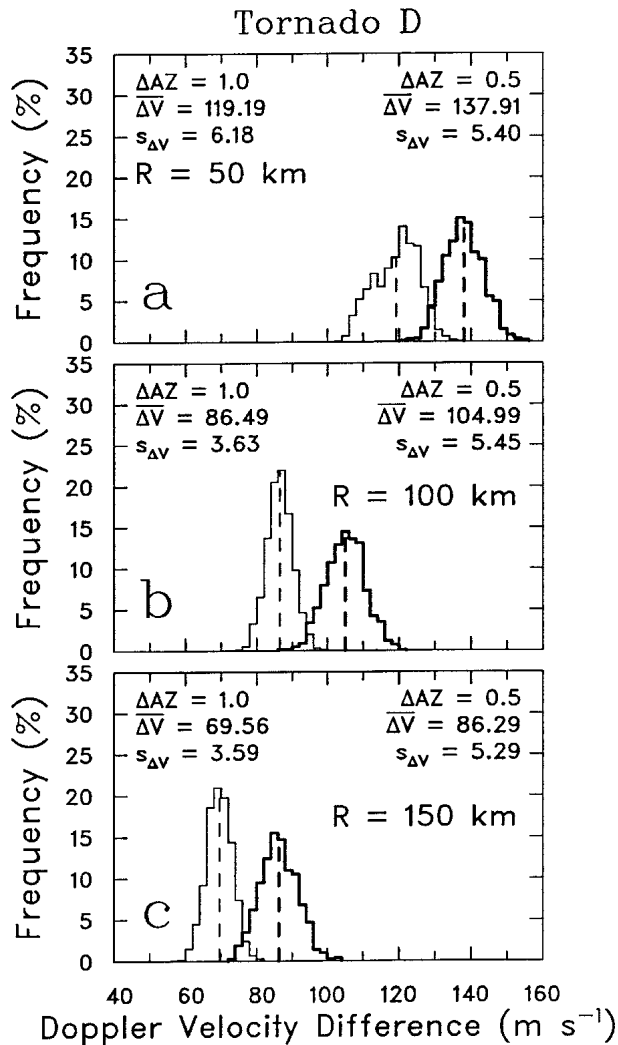


FIG. 6. Same as Fig. 5, except for tornado D (Rankine combined vortex with peak rotational velocity of 100 m s^{-1} and core diameter of 800 m ; after Brown et al. 2002).

pling and those with 1.0° sampling (Fig. 7) for the 2003 tornado situations. Included in the figure are similar data collected during the Oklahoma–Kansas tornado outbreak of 3 May 1999 (Brown et al. 2002). Since many of the tornadoes during April and May 2003 were sampled using scanning strategy A (Table A1), tornado and tornadic vortex signatures could not be resolved at the three lowest elevation angles owing to the low Nyquist interval of 12.4 m s^{-1} . In about 85% of the situations the magnitudes of signatures were stronger using 0.5° sampling, with about 25% of the signatures being at least 15% stronger.

5. Comparisons of reflectivity signatures

Reflectivity signatures in severe storms are more difficult to quantify than Doppler velocity signatures, so

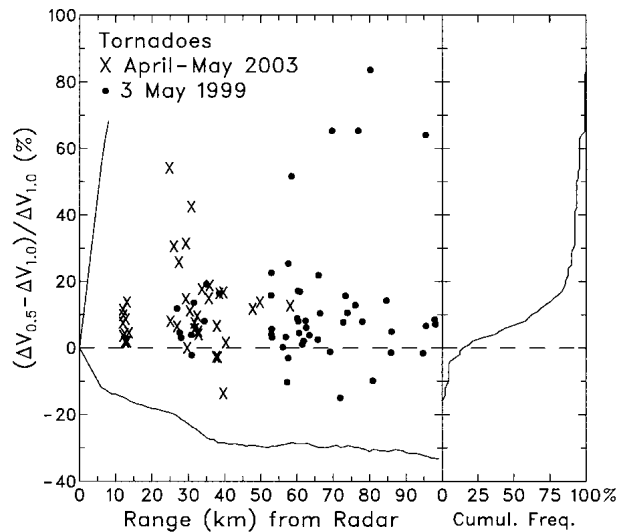


FIG. 7. Percentage differences between Doppler velocity differences (ΔV) from 0.5° -azimuthal data collection and Doppler velocity differences from 1.0° -azimuthal data collection for tornado and tornadic vortex signatures at all elevation angles plotted as a function of range from radar. Each data point represents the percentage difference at a given elevation angle. A total of 39 points are plotted for Apr–May 2003 signatures and 51 points for 3 May 1999 signatures. Upper and lower curves represent likely extreme ratios based on simulations of Brown et al. (2002). Cumulative frequency distribution of number of data points is shown on the right side.

advantages of $0.5^\circ/0.25\text{-km}$ data collection over $1.0^\circ/1.0\text{-km}$ data collection are illustrated by comparing images on reflectivity displays. Since fine-resolution reflectivity data have eight times the spatial density of current WSR-88D reflectivity data (Fig. 1), dramatic improvements can be anticipated.

a. Surface boundaries

On 19 May 2003, a cold front passed southeastward over KOUN and over a topographic ridge to the southwest of the radar (Figs. 8a,b). As the front moved over the ridge, a wave developed along the front and a hailstorm formed at the occluded apex. The fine-resolution image in Fig. 8b shows more spatial continuity in enhanced radar return along the cold front, especially near the growing storm.

During the next 70 min, the storm split into a left-moving storm and a right-moving storm. The gust front associated with the right-moving storm is shown in Figs. 8c and 8d at a range of about 40 km. While the current-resolution display contains the suggestion of a possible gust front, the fine-resolution display shows it very clearly, even though there is more noise in the data. The fine-resolution gust front position was confirmed by fine-resolution Doppler velocity convergence (not shown). Generally, boundaries indicated by fine-resolution data (both reflectivity and Doppler

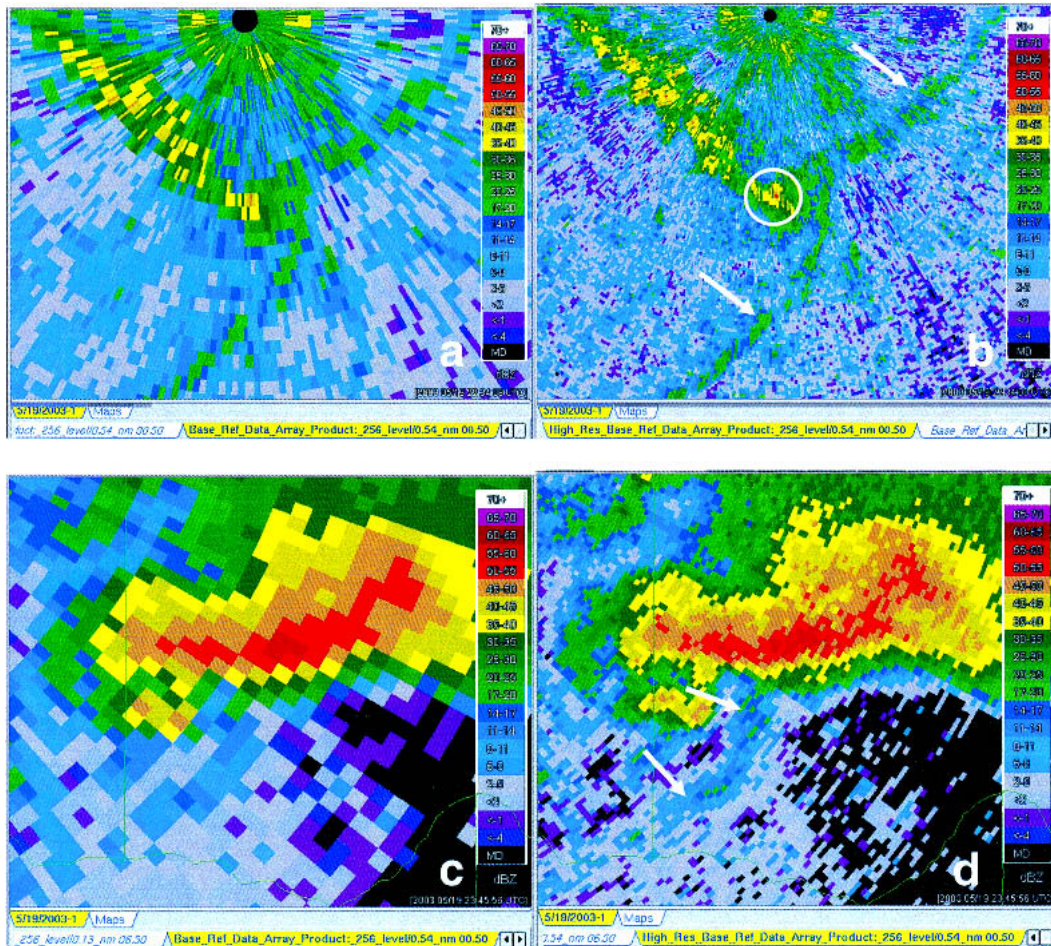


FIG. 8. (left) Current-resolution and (right) fine-resolution reflectivity displays of (a)–(b) a cold frontal boundary at 2234 UTC and (c)–(d) a gust front at 2346 UTC 19 May 2003. The cold frontal boundary [white arrows in (b)] extends from southwest to northeast across the display (0.5° elevation angle). The strong echo (white circle) 13 km due south of the radar (black dot at top) is the beginning of a hailstorm that formed along the cold front as it moved southeastward over the northwest–southeast-oriented ridge (line of yellow and orange echoes). White arrows in (d) indicate location of the gust front associated with a resulting hailstorm located about 40 km southeast of the radar (0.5° elevation angle, 0.45-km height).

velocity) had greater temporal continuity than those provided by current-resolution data. These traits suggest that a combination of fine-resolution reflectivity and fine-resolution Doppler velocity data could be used to improve automated boundary detection algorithms.

b. Bounded weak echo regions

A bounded weak echo region (BWER) is a midaltitude reflectivity minimum that is generally thought to indicate the presence of a strong updraft within a severe thunderstorm. BWERs were detected in different storms at a variety of ranges from KOUN (Fig. 9). A storm at 80-km range (Figs. 9a,b) reveals the presence of a BWER at both resolutions, but the minimum is more pronounced in the fine-resolution display. At 140-

km range (Figs. 9c,d), a BWER is not evident in the current-resolution display, but a BWER is very obvious in the fine-resolution display. Even at a range of 195 km (Figs. 9e,f), the fine-resolution display shows a pronounced BWER while there is only a suggestion of one (an isolated yellow bin) in the current-resolution display. Fine-resolution BWERs are so obvious because minimum reflectivity values are 5–15 dBZ lower than with current resolution.

c. Hook echoes

A hook-shaped reflectivity feature (called a hook echo), that typically is on the right rear flank of a severe storm, indicates the presence of a mesocyclone that has the potential of having a tornado form within it. As such, the hook echo is an important signature that fore-

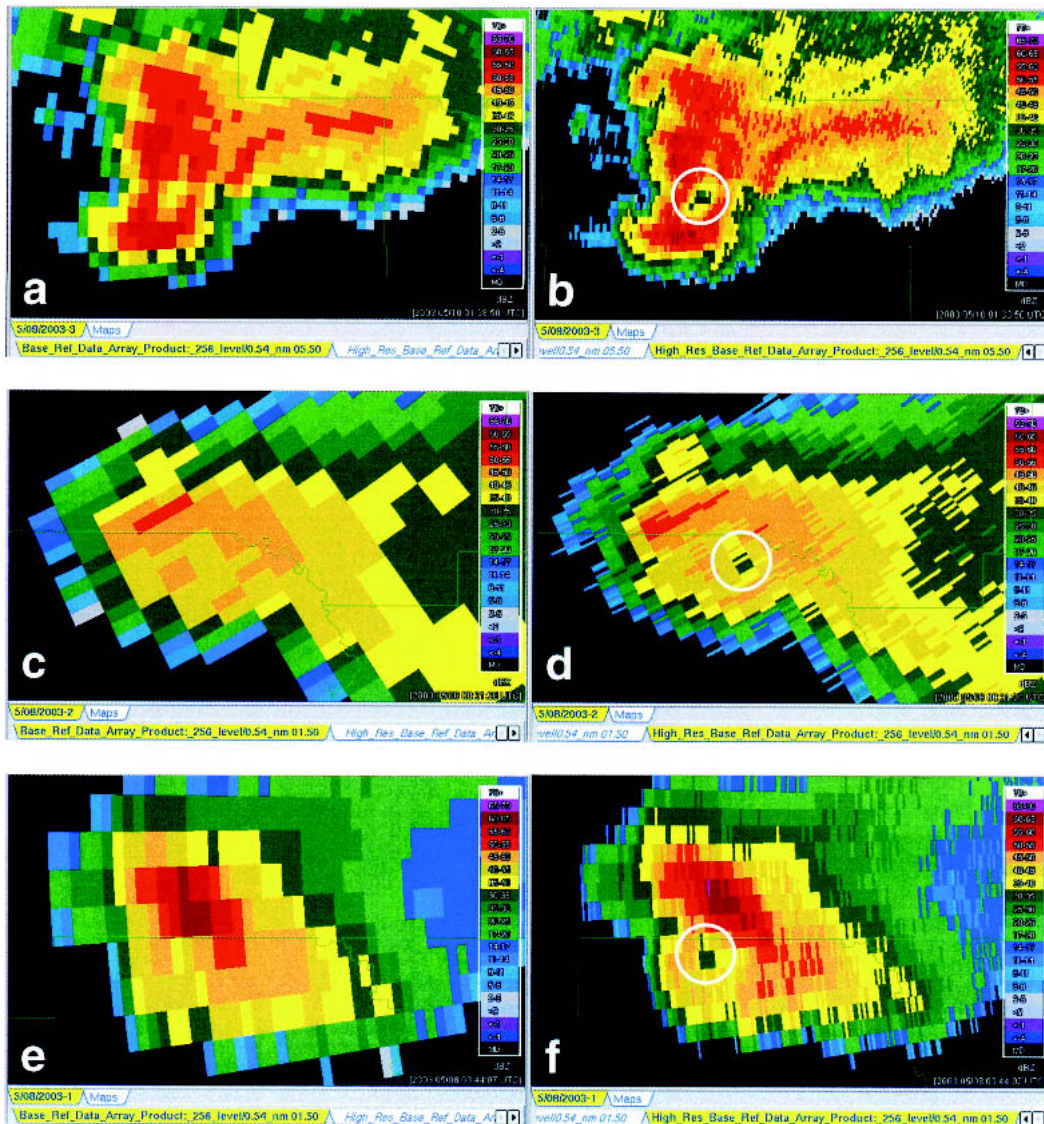


FIG. 9. (left) Current-resolution and (right) fine-resolution reflectivity displays of severe storms containing bounded weak echo regions (inside white circles). (a)–(b) BWER located 80 km west of the radar at a height of 8.3 km (5.5° elevation angle) at 0139 UTC 10 May 2003. (c)–(d) BWER located 140 km south-southeast of the radar at a height of 4.9 km (1.5° elevation angle) at 0831 UTC 8 May 2003. (e)–(f) BWER located 195 km west of the radar at a height of 7.1 km (1.5° elevation angle) at 0344 UTC 8 May 2003. Reflectivity color scales along the right sides of the displays are incremented by 5 dBZ starting with 20–25 dBZ (second green color.).

casters use to indicate the presence of a severe storm. On 8 May 2003, a tornadic storm (that caused F0 damage) occurred at a range of 140 km from the radar. The current-resolution reflectivity field revealed only a subtle suggestion of a hook echo (Fig. 10a). However, the fine-resolution reflectivity field revealed a more obvious indication of a hook echo (Fig. 10b). The fact that the feature was a hook echo was confirmed by the presence of a mesocyclone signature in the Doppler velocity field (not shown).

On 10 May 2003, a more dramatic hook echo occurred only 40 km from the radar (Figs. 10c,d). Being

so close to the radar, the hook was obvious in both the current- and fine-resolution data. At the tip of the hook echo was a region of high reflectivity that the finer-resolution data revealed to be essentially circular. The local reflectivity maximum was the debris cloud rotating around a tornado that was producing F3 damage at that time. Doppler velocity data revealed the presence of a TVS coincident with the debris cloud at the center of the mesocyclonic circulation (Figs. 10e,f). Fine-resolution Doppler velocity data indicated a velocity difference across the TVS of 64 m s^{-1} and current-resolution data indicated a difference of 63 m

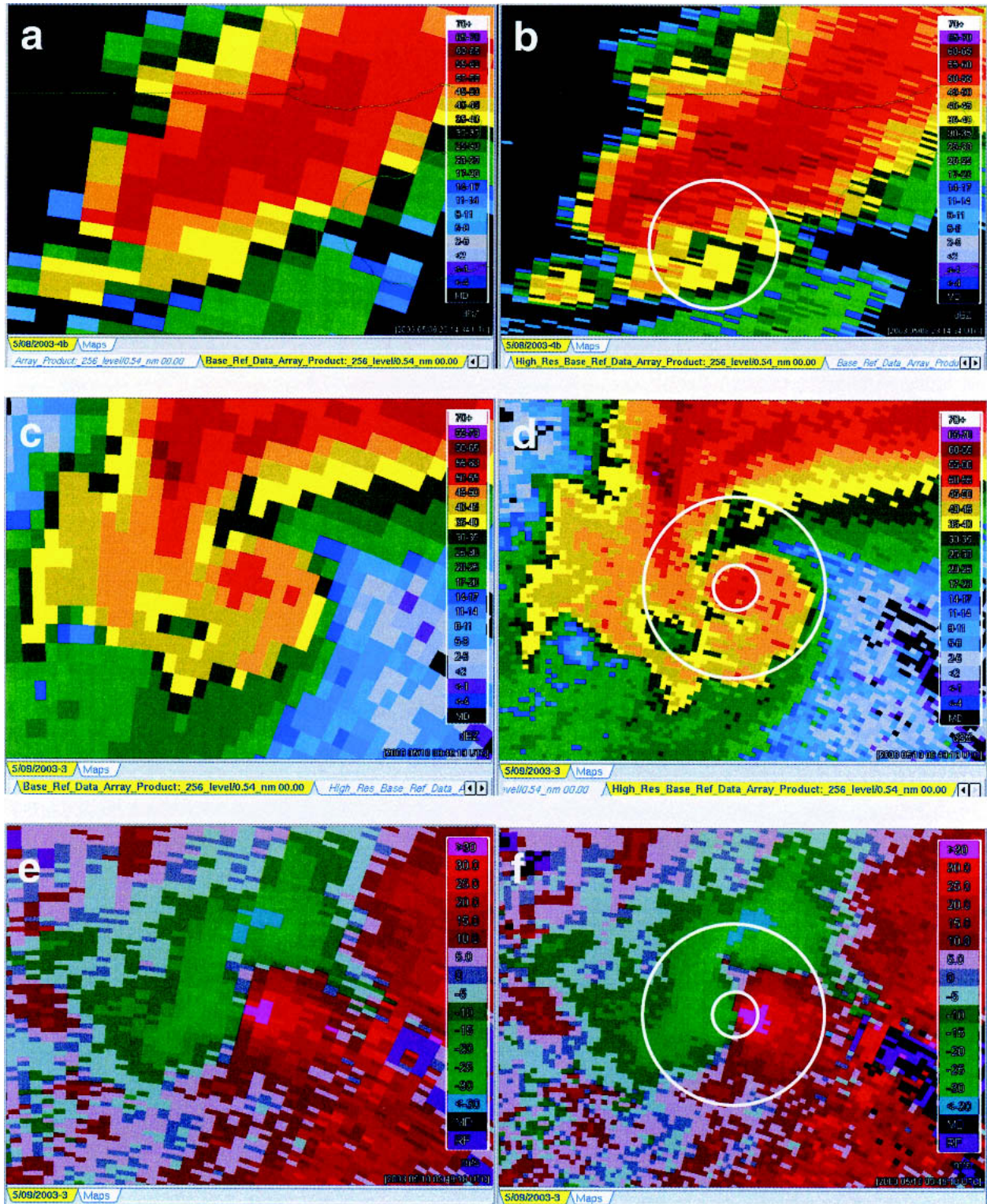


FIG. 10. (left) Current-resolution and (right) fine-resolution reflectivity and Doppler velocity displays of hook echoes/mesocyclones (inside large white circles). (a)–(b) Reflectivity pattern associated with a hook echo at range of 140 km north-northeast of the radar (0.0° elevation angle, 1.2-km height) at 2314 UTC 8 May 2003. (c)–(d) Reflectivity pattern of a hook echo and tornado debris cloud (smaller circle) at range of 40 km north-northeast of the radar (0.0° elevation angle, 0.1-km height) at 0349 UTC 10 May 2003. (e)–(f) Doppler velocity pattern (0.5° elevation angle, 0.45-km height) associated with the reflectivity pattern in (c) and (d); a Doppler velocity display was not available at 0.0° elevation. The smaller white circle indicates the Doppler velocity signature of the tornado that produced the debris echo at the end of the hook echo.

s^{-1} . Dual polarization studies reveal that the debris cloud produces a distinctive polarization signature because the scatterers are large and have irregular shapes (e.g., Schuur et al. 2004).

6. Concluding discussion

We compared displays of current-resolution WSR-88D Doppler velocity and reflectivity signatures in severe storms with displays showing finer-resolution signatures obtained by a test bed WSR-88D. Fine-resolution data were produced by processing data at 0.5° -azimuthal intervals rather than at conventional 1.0° intervals and by using range data at 0.25-km intervals. Consequently, fine-resolution displays have twice the number of Doppler velocity and spectrum width data points and eight times the number of reflectivity data points.

Severe storm characteristics were depicted more clearly with fine-resolution data. Gust fronts and other low-altitude boundaries are more readily identifiable with fine-resolution data. Bounded weak echo regions that may not be evident with current-resolution data can be more obvious with fine-resolution data. Eighty-five percent of mean rotational velocities for fine-resolution mesocyclone signatures were stronger than those for current-resolution signatures. Likewise, 85% of the fine-resolution Doppler velocity differences across tornado and tornadic vortex signatures were stronger. At ranges greater than 100 km, fine-resolution reflectivity displays revealed severe storm signatures, such as bounded weak echo regions and hook echoes, which were not readily apparent on current-resolution displays.

We envision that 0.5° -azimuthal sampling will be achieved operationally by maintaining current antenna rotation rates and using half the number of pulses to compute the radar parameters. Halving the number of pulses produces slightly noisier data because the standard deviation of the parameter estimates increases by $\sqrt{2}$. Full utilization of fine-resolution data would require a technique for reducing the variance of the parameter estimates. One promising technique is the range oversampling and whitening approach proposed by Torres and Zrnić (2003) and evaluated by Ivić et al. (2003). The technique works by oversampling in range—that is, by acquiring many samples within a range cell, and then manipulating these samples such that they become decorrelated. This manipulation is called “whitening.” Decorrelation increases the number of independent samples that in turn decreases the variance of the estimation. However, the whitening process introduces noisiness that reduces the radar system sensitivity. As the number of samples increases, the estimate variance decreases while the introduced noise increases. The operational trade-off is variance reduc-

tion versus radar system sensitivity or, stated another way, data acquisition speed and estimate accuracy versus radar system sensitivity.

For the WSR-88D, oversampling by a factor of 10 provides an estimate variance reduction by a factor of 8 and a noise increase of 10 dB. The effect of the noise increase is noticeable. For example, the minimum detectable rainfall rate at 250 km would increase from 0.0024 to 0.018 in h^{-1} owing to an equivalent noise increase of 14 dB at the 0 dB signal-to-noise ratio associated with the minimum detectable signal. Good performance of the whitening method occurs at about 20 dB above the current WSR-88D noise level. Using these trade-offs, VCPs 11 and 12 could run in 3.6 min, provide full-resolution data (0.5° , 0.25 km) with Doppler velocity standard deviation less than 0.7 m s^{-1} and reflectivity standard deviation less than 0.9 dB for system specifications of large signal-to-noise ratios and input spectrum width of 4 m s^{-1} . This technique is ready for operational evaluation.

In the meantime, there are several other things that must occur before fine-resolution displays become operational. Fine-resolution data cannot be collected until after Open Radar Data Acquisition (ORDA) units are installed at WSR-88D radar sites (e.g., Saffle et al. 2003). To have available both current-resolution and fine-resolution data at the Open Radar Product Generator (ORPG), a decision must be made whether to send both current- and fine-resolution data directly from ORDA to ORPG or to send fine-resolution data from ORDA to ORPG and use the recombination algorithm at ORPG to produce current-resolution data as was done in this study. In either case, with larger quantities of data being sent between ORDA and ORPG, data compression techniques will have to be employed. Initially, fine-resolution data probably would be used only for displays. Current-resolution data would continue to be used for the various meteorological algorithms until the whitening technique becomes available for decreasing estimate variances and until algorithms are modified so they can handle fine-resolution data.

In summary, these findings hold great promise for helping to improve future severe storm warning capabilities for forecasters. The impact of fine-resolution reflectivity measurements—with an eightfold increase in data density—would be enhanced detection of low-altitude boundaries and the identification of severe and tornadic storm signatures (such as hook echoes and bounded weak echo regions) at greater ranges from the radar. The impact of fine-resolution Doppler velocity measurements, with a twofold increase in data density, would be the identification of stronger signatures associated with mesocyclones and tornadoes. Additionally, simulations indicate that signatures can be found up to 50% farther in range. Thus, the principal advantage of fine-resolution measurements over current-resolution

TABLE A1. Scanning strategy A used to collect fine-resolution Doppler radar data with KOUN during spring 2003.

Elevation angle ($^{\circ}$)	Pulse repetition frequency (Hz)	Rotation rate ($^{\circ} \text{ s}^{-1}$)	No. of samples ($0.5^{\circ} \Delta\text{AZ}$)	Nyquist velocity (m s^{-1})	Unambiguous range (km)
0.0	446	9.3	24	12.4	336
0.5	446	9.3	24	12.4	336
1.5	446	9.3	24	12.4	336
2.5	1013	21.0	24	28.1	148
3.5	1013	21.0	24	28.1	148
4.5	1013	21.0	24	28.1	148
5.5	1013	21.0	24	28.1	148
6.5	1013	21.0	24	28.1	148
7.5	1013	21.0	24	28.1	148
8.7	1013	21.0	24	28.1	148
10.0	1013	21.0	24	28.1	148
12.0	1013	21.0	24	28.1	148
14.0	1013	21.0	24	28.1	148
16.6	1013	21.0	24	28.1	148
19.5	1013	21.0	24	28.1	148

measurements is the ability to detect stronger reflectivity and Doppler velocity signatures at greater ranges from a WSR-88D.

Acknowledgments. Data used in this study were collected by “piggybacking” on the spring 2003 Joint Polarization Experiment (JPOLE). We appreciate the willingness of Terry Schuur (NSSL/CIMMS), JPOLE Director, to have scanning strategies modified to collect 0.5° -azimuthal data. Valery Melnikov (NSSL/CIMMS) developed the scanning strategies, and he and Terry Schuur operated KOUN radar during data collection. Chris Curtis and Dan Suppes (NSSL/CIMMS) assisted in various aspects of data processing and archiving. Lulin Song and Robert Toomey (NSSL/CIMMS) corrected WDSS II display problems that became evident during data analysis. Data analyses were supported through a Memorandum of Understanding between the WSR-88D Radar Operations Center and NSSL.

APPENDIX

Experimental Scanning Strategies

The two primary scanning strategies used in this study with NSSL’s test bed radar KOUN are shown in Tables A1 and A2. Unlike WSR-88D scanning strategies, KOUN scanning strategies included a 0.0° elevation angle. Also, KOUN did not make two scans with separate pulse repetition frequencies (PRF) at lower elevation angles. (The separate WSR-88D scans provide a low-PRF long-range reflectivity surveillance scan with no range folding and a high-PRF high-Nyquist-velocity scan with minimal Doppler velocity aliasing.) The three lowest KOUN elevation angles of scanning strategy A (Table A1) and the lowest elevation angle of scanning strategy B (Table A2) used a low PRF that provided long-range reflectivity coverage of storms. However, the corresponding Nyquist velocity was only $\pm 12.4 \text{ m s}^{-1}$, which produced so much Doppler velocity

TABLE A2. Scanning strategy B used to collect fine-resolution Doppler radar data with KOUN during spring 2003.

Elevation angle ($^{\circ}$)	Pulse repetition frequency (Hz)	Rotation rate ($^{\circ} \text{ s}^{-1}$)	No. of samples ($0.5^{\circ} \Delta\text{AZ}$)	Nyquist velocity (m s^{-1})	Unambiguous range (km)
0.0	446	9.3	24	12.4	336
0.5	1282	20.0	32	35.5	117
1.5	1282	20.0	32	35.5	117
2.5	1282	20.0	32	35.5	117
3.5	1282	20.0	32	35.5	117
4.5	1282	20.0	32	35.5	117
5.5	1282	20.0	32	35.5	117
6.5	1282	20.0	32	35.5	117
7.5	1282	20.0	32	35.5	117
8.7	1282	20.0	32	35.5	117
10.0	1282	20.0	32	35.5	117
12.0	1282	20.0	32	35.5	117
14.0	1282	20.0	32	35.5	117
16.6	1282	20.0	32	35.5	117
19.5	1282	20.0	32	35.5	117

aliasing that it was extremely difficult, if not impossible, to properly interpret Doppler velocity displays of mesocyclone and, especially, tornadic vortex signatures at those elevation angles.

REFERENCES

- Brown, R. A., L. R. Lemon, and D. W. Burgess, 1978: Tornado detection by pulsed Doppler radar. *Mon. Wea. Rev.*, **106**, 29–38.
- , V. T. Wood, and D. Sirmans, 2002: Improved tornado detection using simulated and actual WSR-88D data with enhanced resolution. *J. Atmos. Oceanic Technol.*, **19**, 1759–1771.
- , R. M. Steadham, B. A. Flickinger, and V. T. Wood, 2003: A new WSR-88D scanning strategy: Results of field tests. Preprints, *31st Conf. on Radar Meteorology*, Seattle, WA, Amer. Meteor. Soc., 960–963.
- Curtis, C. D., S. M. Torres, and E. Forren, 2003: High-resolution WSR-88D base data on the KOUN research radar. Preprints, *31st Conf. on Radar Meteorology*, Seattle, WA, Amer. Meteor. Soc., 964–966.
- Heiss, W. H., D. L. McGrew, and D. Sirmans, 1990: NEXRAD: Next Generation Weather Radar (WSR-88D). *Microwave J.*, **33**, 79–80, 84–98.
- Hondl, K. D., 2002: Current and planned activities for the Warning Decision Support System—Integrated Information (WDSS-II). Preprints, *21st Conf. on Severe Local Storms*, San Antonio, TX, Amer. Meteor. Soc., 146–148.
- Ivić, I. R., D. S. Zrnić, and S. M. Torres, 2003: Whitening in range to improve weather radar spectral moment estimates. Part II: Experimental evaluation. *J. Atmos. Oceanic Technol.*, **20**, 1449–1459.
- Saffle, R. E., R. C. Elvander, and M. J. Istok, 2003: NEXRAD product improvement—Expanding science horizons. Preprints, *31st Conf. on Radar Meteorology*, Seattle, WA, Amer. Meteor. Soc., 956–959.
- Schuur, T. J., A. V. Ryzhkov, P. L. Heinselman, D. W. Burgess, and K. A. Scharfenberg, 2004: The Joint Polarization Experiment—A summary of dual-polarization WSR-88D radar data collection and analysis. Preprints, *20th Conf. on Interactive Information Processing Systems*, Seattle, WA, Amer. Meteor. Soc., CD-ROM, 12.1.
- Torres, S. M., and D. S. Zrnić, 2003: Whitening in range to improve weather radar spectral moment estimates. Part I: Formulation and simulation. *J. Atmos. Oceanic Technol.*, **20**, 1433–1448.
- Wood, V. T., R. A. Brown, and D. Sirmans, 2001: Technique for improving detection of WSR-88D mesocyclone signatures by increasing angular sampling. *Wea. Forecasting*, **16**, 177–184.